Dalton Transactions

Accepted Manuscript

ROYAL SOCIETY OF CHEMISTRY

www.rsc.org/dalton

Dalton Trans, 2014, revised 19332614_File000003_410109473.docx

Manganese Borohydride; Synthesis and Characterization

Bo Richter[1], Dorthe B. Ravnsbæk[1,2], Nikolay Tumanov[3], Yaroslav Filinchuk[3], Torben R. Jensen[1,*]

[1] Interdisciplinary Nanoscience Center (iNANO) and Department of Chemistry, University of Aarhus, Langelandsgade 140, DK-8000 Aarhus C, Denmark.

[2] Department of Material Science and Engineering, Massachusetts Institute of Technology, 77 Massachusetts Avenue, Cambridge 02139, Massachusetts.

[3] Institute of Condensed Matter and Nanosciences, Université Catholique de Louvain, place L. Pasteur 1, B-1348 Louvain-la-Neuve, Belgium.

* To whom correspondence should be addressed. T. R. J. (trj@chem.au.dk).

Dalton Trans, 2014, revised 19332614_File000003_410109473.docx

ABSTRACT

Solvent-based synthesis and characterization of α-$Mn(BH_4)_2$ and a new nanoporous polymorph of manganese borohydride, γ-$Mn(BH_4)_2$, via a new solvate precursor, $Mn(BH_4)_2{\cdot}½S(CH_3)_2$, is presented. Manganese chloride is reacted with lithium borohydride in a toluene/dimethylsulfide mixture at room temperature, which yields halide and solvent-free manganese borohydride after extraction with dimethylsulfide (DMS) and subsequent removal of residual solvent. This work constitutes the first example of establishing a successful, reproducible solvent-based synthesis route for a pure, crystalline, stable transition metal borohydride. The new polymorph, γ-$Mn(BH_4)_2$, is shown to be the direct manganese counterpart of the zeolite-like structure, γ-$Mg(BH_4)_2$ (cubic, a = 16.209(1) Å, space group *Id*-3*a*). It is verified that large pores (diameter > 6.0 Å) exist in this structure. The solvate, $Mn(BH_4)_2{\cdot}½S(CH_3)_2$, is subsequently shown to be the analogue of $Mg(BH_4)_2{\cdot}½S(CH_3)_2$. As the structural analogies between $Mg(BH_4)_2$ and $Mn(BH_4)_2$ became evident a new polymorph of $Mg(BH_4)_2$ was identified and termed ζ-$Mg(BH_4)_2$. ζ-$Mg(BH_4)_2$ is the structural counterpart of α-$Mn(BH_4)_2$. All synthesis products are characterized employing synchrotron radiation-powder X-ray diffraction, infrared spectroscopy and thermogravimetric analysis in combination with mass spectroscopy. Thermal analysis reveals the decomposition of $Mn(BH_4)_2$ to occur at 160 °C, accompanied by a mass loss of 14.8 wt%. A small quantity of the desorbed gaseous species is identified as diborane ($\rho_m(Mn(BH_4)_2)$ = 9.5 wt% H_2), while the remaining majority is found to be hydrogen.

Keywords: Hydrogen storage materials, manganese borohydride, magnesium/manganese borohydride, isopolymorphism, borohydride synthesis.

Dalton Trans, 2014, revised 19332614_File000003_410109473.docx

INTRODUCTION

The increasing world-wide energy demand necessitates still new approaches for implementing safe and environmentally benign forms of energy, to replace fossil fuels [1]. Current research efforts within hydrogen storage focus on high storage densities, prolific thermodynamic and kinetic properties and reversibility, to allow renewable energy storage for mobile applications [2]. The current technology utilizes high pressure hydrogen tanks; e.g. $p(H_2) \sim 700$ bar for the automotive industry [3]. As an alternative to pressure tanks, solid state chemical storage of hydrogen is being investigated. For example, utilization of hydride materials to act as solid state storage media for renewable energy is intensely studied. Several classes of materials are investigated, such as metal alloys, magnesium based hydrides and metal borohydrides [3-6]. The latter exhibit fascinating characteristics, both structurally and chemically [7-9]. Borohydrides hold high hydrogen contents; however release of hydrogen is achieved under less than favorable conditions and in certain cases undesired release of diborane poses a challenge [10, 11], and they often suffer from slow kinetics. A well-known example is $LiBH_4$, holding 18.4 wt% hydrogen, unfortunately being considerably hampered by its enthalpy of decomposition (-67 kJ/mol). Several methods for improving the hydrogen storage properties of such compounds exists [12]; formation of reactive hydride composites (RHC's) [13, 14], incorporation into nanoporous carbon scaffolds (nano confinement) [15, 16], anion substitution [4, 18] and formation of bi-metallic materials [19, 20]. However, so far synthesis of the ideal hydrogen storage material based on borohydrides has not been achieved. Rehydrogenation of the storage materials is another challenge. Hydrogen pressure of 950 bar and 400 ^oC have been shown to hydrogenate MgB_2 to $Mg(BH_4)_2$ over several days [21], but this is no practical solution. Among transition metal borohydrides [22-26], manganese borohydride is an interesting candidate owing to its reportedly low temperature of decomposition [27, 28]. Unfortunately, thermal decomposition of $Mn(BH_4)_2$ is accompanied with the liberation of hydrogen,

but also some diborane [27]. Reactive manganese borohydride – metal hydride composites may be designed to suppress the release of diborane [29]. Bimetallic borohydrides, e.g. $LiZn_2(BH_4)_5$, releases a hydrogen-diborane mixture of approximately 1:1 composition, and has even been used as an indirect source of diborane [30]. Preceding work on $Mn(BH_4)_2$, employing solvent based synthesis routes, provided tetrahydrofuran (THF) adducts. However, pure $Mn(BH_4)_2$ could not be extracted due to the high temperatures needed to remove THF, causing the borohydride to decompose [31]. A mechanochemical approach afforded non-crystaline materials, which by spectroscopic methods proved to be a mixed cation manganese borohydride [28]. The first structural characterization of α-$Mn(BH_4)_2$ prepared from a mechanochemical metathesis reaction between $MnCl_2$ and $LiBH_4$, was presented recently [32]. However, the synthesis product, α-$Mn(BH_4)_2$, contains LiCl and thus calls for new methods. For researchers to tailor materials properties fulfilling the demands of solid state hydrogen storage, high purity chemicals are needed. Furthermore, providing new synthesis routes gives important insight into the reaction pathways and properties of the materials in question. In this work we present the synthesis of a new solvate and two polymorphs of $Mn(BH_4)_2$, obtained as halide- and solvent free products.

EXPERIMENTAL SECTION

Synthesis. 2.52 g (20.0 mmol, 1.33 equivalents, 33% excess) finely ground $MnCl_2$ (Aldrich, ≥99%, anhydrous) was suspended in an 80:20 toluene-dimethylsulfide mix (50 mL) (anh., Sigma-Aldrich) at room temperature. Two equivalents (0.65 g, 30 mmol) of finely ground $LiBH_4$ (Sigma-Aldrich, ≥98%) was added to the pink $MnCl_2$ suspension at room temperature, left stirring and shortly after a pale yellow solid formed. The reaction mixture was left stirring at room temperature overnight, turning into a more homogenous and progressively more yellow suspension as stirring proceeded. The mixture was filtered using a finely porous glass filter, and the pale yellow

solid was collected. The collected products, composing a mixture of LiCl and $Mn(BH_4)_2 \cdot ½S(CH_3)_2$, was extracted with dimethylsulfide (DMS) (anh., Sigma-Aldrich, ≥99.0%), and filtered, after which the resulting clear yellow solution was evaporated under pressure, providing firstly a viscous yellow oil, followed by solid $Mn(BH_4)_2 \cdot ½S(CH_3)_2$ as the only product. Subsequent heating under vacuum (110 °C/$2 \cdot 10^{-2}$ mbar) for 16-24 h provided α-$Mn(BH_4)_2$. Collecting the viscous oil before it is solidified, and subsequently drying it under vacuum at *RT* for 3 days provides γ-$Mn(BH_4)_2$ (with traces of α-$Mn(BH_4)_2$). All manipulation of solids are performed in an argon filled glovebox (O_2/H_2O < 0.1 ppm) equipped with a circulation purifier. All manipulation of solvents and solutions are performed using argon as protective atmosphere and inert syringe handling techniques in standard Schlenk glass equipment.

Synchrotron Radiation Powder X-ray Diffraction (SR-PXD)

SR-PXD data were collected at ***a)*** BM01A at the Swiss-Norwegian Beamlines (SNBL) at the European Synchrotron Radiation Facility (ESRF), Grenoble, France and ***b)*** at the synchrotron MAX-II, Lund, Sweden in the research laboratory MAX-lab, beamline I711.

a) SR-PXD at SNBL. The samples were ground in a mortar and mounted in glass capillaries (o.d. 0.5 mm) sealed with glue inside an argon-filled glovebox with a circulation purifier ($p(O_2, H_2O)$ < 0.1 ppm). The 2D powder data were recorded using a MAR345 Imaging Plate detector and a selected wavelength of 0.6967 Å. For all measurements the capillaries were oscillated by 30° during exposure to the X-ray beam for 30 s, followed by a readout time of ~83 s. At *RT* single PXD patterns were collected at three different sample-to-detector distances 150, 250 and 390 mm in order to obtain both data at high diffraction angle and data with higher resolution at low diffraction angles. Subsequently, the sample was heated from *RT* to 200 °C at a rate of 2 °C/min, while SR-PXD data were collected. The temperature was controlled with the Oxford Cryostream 700+. The *in situ* data were collected using a sample-to-detector distance of 390 mm.

b) In situ SR-PXD at MAX-lab. The powdered sample was mounted in a sapphire (Al_2O_3) single crystal tube (o.d. 1.09 mm, i.d. 0.79 mm) in an argon-filled glovebox $p(O_2, H_2O) < 1$ ppm. The tube was attached to a specially developed sample cell designed for studies of gas/solid reactions and allowing for high pressures and temperatures to be applied. During heating the temperature was controlled with a thermocouple placed in the sapphire tube ~1 mm from the sample [33]. A heating rate of 5 ^oC/min was applied up to temperatures of 300 ^oC, while vacuum, argon atmosphere (p(Ar) = 1 bar) or hydrogen pressure ($p(H_2)$ = 10 bar) was applied to the samples. SR-PXD data was collected by a MAR165 CCD detector system using X-ray exposure time of 30 s and selected wavelengths of λ = 0.9920, 1.0096 or 1.0080 Å [34, 35]. The FIT2D program [36] was used for calibrating the wavelengts using a standard (NIST) LaB_6 sample, masking diffraction spots from the single crystal sapphire sample holder and transforming all obtained raw images from both SNBL and MAX-lab to 2D-powder patterns. Uncertainties of the integrated intensities were calculated at each 2θ-point by applying Poisson statistics to the intensity data, considering the geometry of the detector [37].

Structural Refinement by the Rietveld method

Rietveld refinement was carried out using the program FullProf [38]. In general, backgrounds were described by linear interpolation between selected points. For all structures scale-factors, cell parameters, profile parameters and overall displacement factor, B_{ov} were refined as a minimum. Furthermore, zero-shift was refined for all data. Note that the high χ^2 values reflect mainly the extremely high counting statistics of the powder diffraction data obtained from modern 2D-detectors. The structure of $Mn(BH_4)_2 \cdot ½S(CH_3)_2$ was refined by simultaneous Rietveld refinement of two SR-PXD data sets measured on the same sample at SNBL at *RT* with a sample-to-detector distance of 150 and 390 mm, respectively to take full advantage of both high angle data (150 mm dataset) and high resolution at low angle (390 mm dataset). Two sets of Bragg reflections were

identified in the data, one was assigned to α-$Mn(BH_4)_2$ [32] while the other set of reflections were recognized as being similar to the diffraction pattern for $Mg(BH_4)_2 \cdot ½S(CH_3)_2$. Hence, Mn was substituted for Mg in the monoclinic structural model for $Mg(BH_4)_2 \cdot ½S(CH_3)_2$ (space group *Cc*) as presented in ref. [39] and this was used as starting model for the refinement together with the structural data for $Mn(BH_4)_2$ as given in ref. [32]. For $Mn(BH_4)_2 \cdot ½S(CH_3)_2$ all atomic positions were refined using 40 distance restraints for interatomic distances and 37 for angles. Only positions (not the orientation) of the CH_3 and BH_4 units were refined. As for the displacement factors, those for $Mg(BH_4)_2 \cdot ½S(CH_3)_2$ [39] were used as starting points and the displacements factors were refined for freely for Mn and S while those for the CH_3 and BH_4 groups were refined together. The final discrepancy factors for the 150 and 390 mm datasets are: χ^2 = 1360 and 1450, R_{wp} = 0.913 and 1.99 % (not corrected for background), R_p = 2.38 and 4.28 % (corrected for background), $R_B(Mn(BH_4)_2 \cdot ½S(CH_3)_2)$ = 1.03 and 1.29 % and R_B ($Mn(BH_4)_2$) = 1.64 and 2.55 %. The refinement profiles are shown in Fig. S2.1. Crystal data and atomic coordinates are listed in Table S2.1. The structure of γ-$Mn(BH_4)_2$ was refined from SR-PXD data (MAX-lab, λ = 0.9920 Å) measured at *RT*. One set of Bragg reflections in the data was assigned to γ-$Mn(BH_4)_2$ (being similar to the diffraction pattern for γ-$Mg(BH_4)_2$ [39]). Hence, Mn was substituted for Mg in the structural model for γ-$Mg(BH_4)_2$ (space group *Id*-3*a*) and this was used as starting point for the refinement. Reflections from a small amount of α-$Mn(BH_4)_2$ was refined from the model for $Mn(BH_4)_2$ as given in ref. [32]. Furthermore, the SR-PXD data contains reflections (see supporting info for *d*-spacings) from one or more unidentified compounds, which may a manganese analogue of ε-$Mg(BH_4)_2$ as described in ref. [40]. However, the small amount and the low number of Bragg peaks hamper indexing as well as comparison with published data. For γ-$Mn(BH_4)_2$, Mn is located on a special position, hence only positions (not the orientation) of the BH_4 units were refined. The final discrepancy factors are: χ^2 = 21.51, R_{wp} = 5.95 % (not corrected for background), R_p = 25.7 % (corrected for background), R_B(γ-

$Mn(BH_4)_2$) = 14.8 %. The fact that undescribed reflections remain in the refinement is clearly seen from the relatively high agreement factors. The refinement profiles are shown in Fig. S2.2. Crystal data and atomic coordinates are listed in Table S2.2.

The structure of ζ-$Mg(BH_4)_2$ was refined from SR-PXD data (SNBL, ESRF, λ = 0.7035 Å) measured at 224 °C. Realizing that the diffraction pattern of ζ-$Mg(BH_4)_2$ is similar to that of α-$Mn(BH_4)_2$ (space group $P3_112$) [32], allowed to develop a structural model for ζ-$Mg(BH_4)_2$ by substitution of Mg for Mn, which was used as starting point for the refinement. The refinement profiles are shown in Fig. S2.3. Due to the quality of the data, the BH_4 units were refined as rigid bodies and only positions (not orientations) of the tetrahedra were refined, and individual displacement factors were not refined. The final discrepancy factors are: $\chi^2 = 21.5$, $R_{wp} = 0.420$ % (not corrected for background), $R_p = 25.1$ % (corrected for background), R_B(ζ-$Mg(BH_4)_2$) = 13.6 %.

Thermal analysis, TGA-DSC/TPD-MS. Thermogravimetric analysis (TGA) and differential scanning calorimetry (DSC) were collected for $Mn(BH_4)_2 \cdot ½S(CH_3)_2$ and α-$Mn(BH_4)_2$ using a Perkin-Elmer STA 6000 instrument coupled to a Hiden HPR 20 QIC mass spectrometer (MS) via a heated capillary. The atomic mass ranges probed were set up to detect all fragments of dimethylsulfide, diborane and hydrogen respectively. The measurements were performed in a continuous flow of Ar (65 mL/min) using Al_2O_3 crucibles fitted with a lid to prevent exposure to air when mounted. Gases produced from the decomposition during heating were led through a small hole in the lid and through the inlet of the MS probe. The heating rate was 5 ^oC/min until reaching 250 ^oC.

Infrared Spectroscopy. Infrared spectra were collected by Attenuated Total Reflectance - Fourier Transformed Infrared Spectroscopy (ATR-FTIR), using a Nicolet 380 Avatar spectrometer. The sample powder was placed directly on the infrared radiation source and immediately covered by a tight screw. The total exposure of the materials to air is limited to a few

seconds in this manner. The spectra were collected in the wavenumber range of 4000 - 400 cm^{-1} with 32 scans.

RESULTS AND DISCUSSION

Synthesis. The method utilized for synthesis of $Mn(BH_4)_2$ is a solvent based metathesis reaction, usually performed mechanochemically [41, 42]. The present approach requires no ball milling or activation such as heating or high pressures, i.e. finely ground $MnCl_2$ and $LiBH_4$ (filtered through 112 μm sieves) suspended in toluene/DMS react according to scheme 1 below.

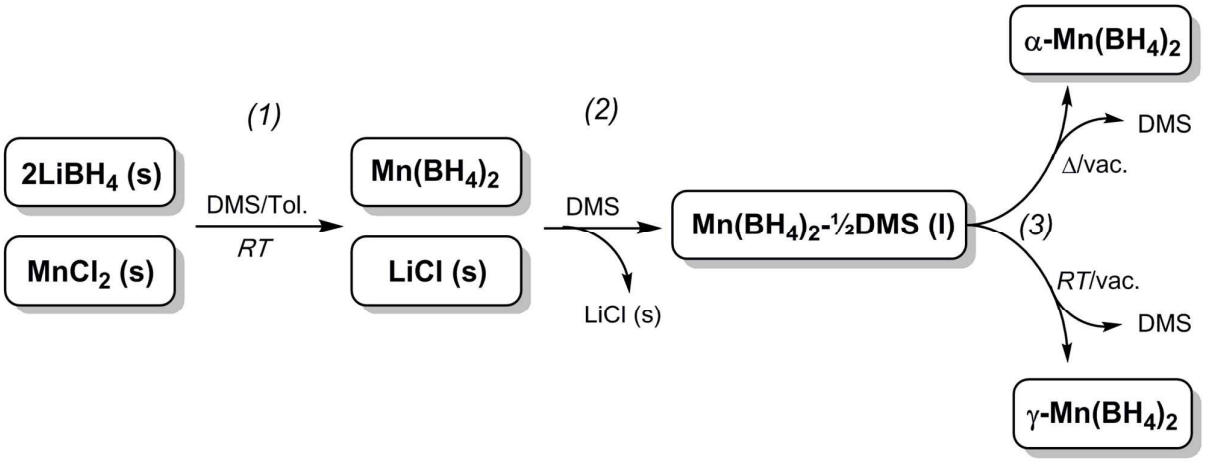

Scheme 1. Reaction scheme for the synthesis of $Mn(BH_4)_2$. *(1)* Metathesis reaction, *(2)* extraction and *(3)* desolvation of $Mn(BH_4)_2 \cdot ½S(CH_3)_2$ yields γ-$Mn(BH_4)_2$ and α-$Mn(BH_4)_2$.

In this manner formation of ternary chlorides, e.g. Li- or NaMn-chlorides, or bi-metallic borohydrides, previously reported to form mechanochemically from $MnCl_2$ and $LiBH_4$ or $NaBH_4$, is avoided [43, 44]. Dimethylsulfide (DMS) as co-solvent and extraction solvent has several advantages. Firstly, the reaction is allowed to proceed faster as the products are being dissolved in DMS as it forms. Secondly, it eliminates the problem of strong coordination of the metal cation to donor (sulfur in DMS) atoms in certain coordinating solvents, i.e. circumventing the problem of

removing e.g. tetrahydrofuran (THF) [31]. Thirdly, the materials are separated from any unreacted starting materials and byproducts (i.e. LiCl) formed during the reaction, since only $Mn(BH_4)_2$ is dissolved as shown in scheme 1. After removing excess DMS, the product obtained is a hard, yellowish powder of $Mn(BH_4)_2{\cdot}½S(CH_3)_2$ (Figure S1.1). Manganese in $Mn(BH_4)_2{\cdot}½S(CH_3)_2$ coordinates relatively weakly to sulfur, thus the solvent can be removed under mild conditions. The coordination is broken at temperatures low enough to preserve the $Mn(BH_4)_2$ (T < 110 °C), in contrast to earlier attempts of desolvating $Mn(BH_4)_2{\cdot}3THF$, where temperatures required (T > 140 °C) were high enough that decomposition occurred [31]. In contrast, subjecting the diethylether magnesium borohydride complex to a longer drying process [45], diethylether can be extracted at T > 180 °C providing the high temperature polymorph β-$Mg(BH_4)_2$ [46]. For these reasons neither diethylether nor THF was used as solvent in this work. Furthermore, diethylether has some solubility of LiCl and $LiBH_4$, which may contaminate the reaction product [47, 48]. The weak coordination of DMS to manganese in $Mn(BH_4)_2{\cdot}½S(CH_3)_2$ is specifically demonstrated by the formation of γ-$Mn(BH_4)_2$, which is a new nanoporous compound, arising from the gentle (vac/*RT*) removal of DMS molecules from the cavities (see the structural discussion below). After desolvation, γ-$Mn(BH_4)_2$ is obtained as a yellowish, sometimes brown powder.

New synthesis methods, which provide halide free metal hydrides for consideration for solid-state hydrogen storage is of significant interest. Recently, yttrium and gadolinium borohydrides were prepared using dimethyl sulfide as a solvent providing new solvates as intermediates, $M(BH_4)_3S(CH_3)_2$ (M = Y or Gd), which transformed to α-$Y(BH_4)_3$ or $Gd(BH_4)_3$ at ~140 °C [49]. Other halide free rare earth metal borohydrides, $Eu(BH_4)_2$ and $Sm(BH_4)_2$, are prepared by a metathesis reaction of trivalent metal chlorides and $LiBH_4$ in ethereal solution, combined with solvent extraction using dimethyl sulfide [50].

Dalton Trans, 2014, revised 19332614_File000003_410109473.docx

Crystal Structures of $Mn(BH_4)_2 \cdot ½S(CH_3)_2$ and γ-$Mn(BH_4)_2$.

The solvate, $Mn(BH_4)_2 \cdot ½S(CH_3)_2$ crystallizes in a monoclinic unit cell, a = 7.6914(4), b = 13.8731(8), c = 12.4278(7) Å and ß = 103.973(4)° (V = 1286.84(13) Å^3, Z = 4), space group *Cc*. The 3D framework of $Mn(BH_4)_2 \cdot ½S(CH_3)_2$ contains two Mn atoms: one (Mn2) is tetrahedrally coordinated to four BH_4 groups, while the other (Mn1) coordinates to four BH_4 groups and one $S(CH_3)_2$ ligand to form a trigonal bipyramid (Figure 1). Each BH_4 unit is coordinated by two Mn atoms. The Mn-B distances within the $[Mn(BH_4)_4]$-tetrahedra range from 2.360(6) to 2.533(7) Å while angles range from 97.51(15) to 128.0(2)°. The Mn-S coordination distance in the $[Mn(BH_4)_4(S(CH_3)_2)]$-trigonal bipyramid is 2.705(9) Å, while Mn-B distances range from 2.451(7) to 2.603(8) Å, which is somewhat longer than those observed within the $[Mn(BH_4)_4]$-tetrahedra in accordance with the increase in coordination number. B-Mn-B angles are within 90.7(3) to 119.3(2)°. Further information can be found in the supporting information. The unit cell volume of $Mn(BH_4)_2 \cdot ½S(CH_3)_2$ is only slightly larger (~1 %) than that of the isostructural magnesium analogue $Mg(BH_4)_2 \cdot ½S(CH_3)_2$ [39]. The desolvated γ-$Mn(BH_4)_2$ crystallizes in the high symmetry cubic space group *Ia*-3*d* with unit cell parameters a = 16.2094(13) Å (V = 4258.93(60) Å^3, Z = 24). The structure consists of a 3D framework build from a single Mn atom tetrahedrally coordinated to four BH_4 units and each BH_4 unit bridges two Mn atoms. The framework has large permanent pores and represents the second only example of porous borohydrides (isostructural to γ-$Mg(BH_4)_2$). The Mn-B distance is 2.483(17) Å, while the B-Mn-B angles with the tetrahedral ranges from 100.70(3) to 128.95(2)° and that between neighboring tetrahedra is 176.30(2)°. The unit cell volume of γ-$Mn(BH_4)_2$ is ~8.8 % larger than the Mg-counterpart [39], which corresponds well with the radius of Mn^{2+}(hs) being larger than that of Mg^{2+}. For both structures Mn-H distances cannot be determined unambiguously because of the limited accuracy of the $[BH_4]$-tetrahedra orientation. However, the refinement of BH_4 positions suggests Mn-H distances ranging from 2.034(8) to 2.211(6) Å.

Dalton Trans, 2014, revised 19332614_File000003_410109473.docx

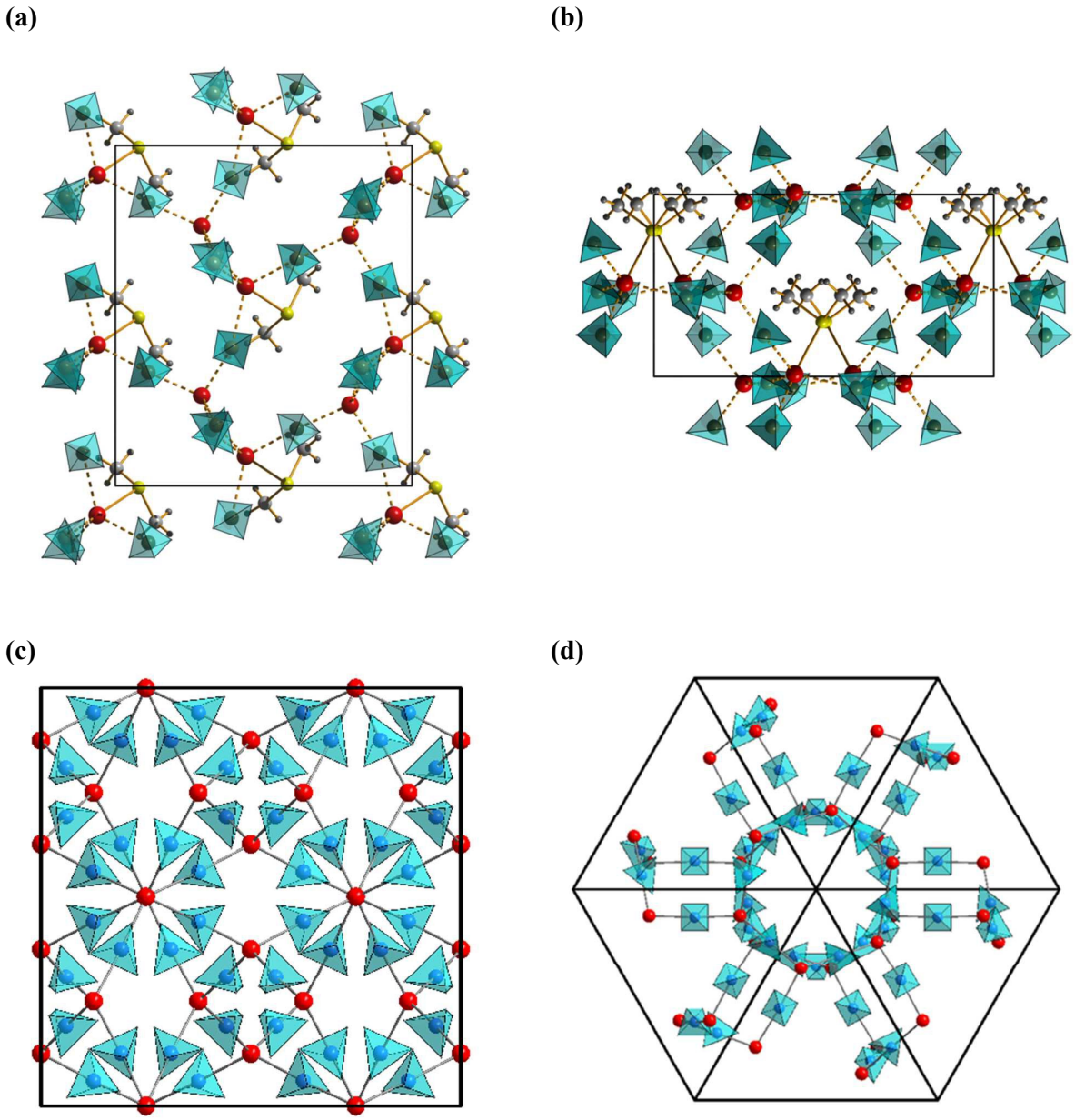

Figure 1. Crystal structure of $Mn(BH_4)_2 \cdot ½S(CH_3)_2$ viewed along the (a) *a*- and (b) *c*-axis and the structure of γ-$Mn(BH_4)_2$ viewed along (c) the *a*-axis and (d) [111]. M-H bonds are omitted for clarity and Mn-B coordinations are shown instead (Mn: red, S: yellow, C: light gray, H: gray, BH_4: blue tetrahedra).

Comparison of $Mn(BH_4)_2$ and $Mg(BH_4)_2$.

α-$Mn(BH_4)_2$ was reported as being structurally similar to $Mg(BH_4)_2$ [32]. We have shown that $Mn(BH_4)_2 \cdot ½S(CH_3)_2$ and $Mg(BH_4)_2 \cdot ½S(CH_3)_2$ are isostructural, and as a consequence hereof we have discovered γ-$Mn(BH_4)_2$, which is structurally identical to the porous zeolite-like γ-$Mg(BH_4)_2$ [39]. Furthermore, we show that α-$Mn(BH_4)_2$ is isostructural to another new $Mg(BH_4)_2$ polymorph, denoted ζ-$Mg(BH_4)_2$ [51]. On the basis of this observation, we have used the Rietveld refinement method to refine X-ray data obtained for the ζ-$Mg(BH_4)_2$ polymorph. Structural and experimental details for $Mg(BH_4)_2$ can be found in Table 1 and in the Supporting Information respectively. In figure 2 (left) the diffraction patterns for ζ-$Mg(BH_4)_2$, γ-$Mg(BH_4)_2$, $Mg(BH_4)_2 \cdot ½S(CH_3)_2$ and its manganese counterparts (right) are shown.

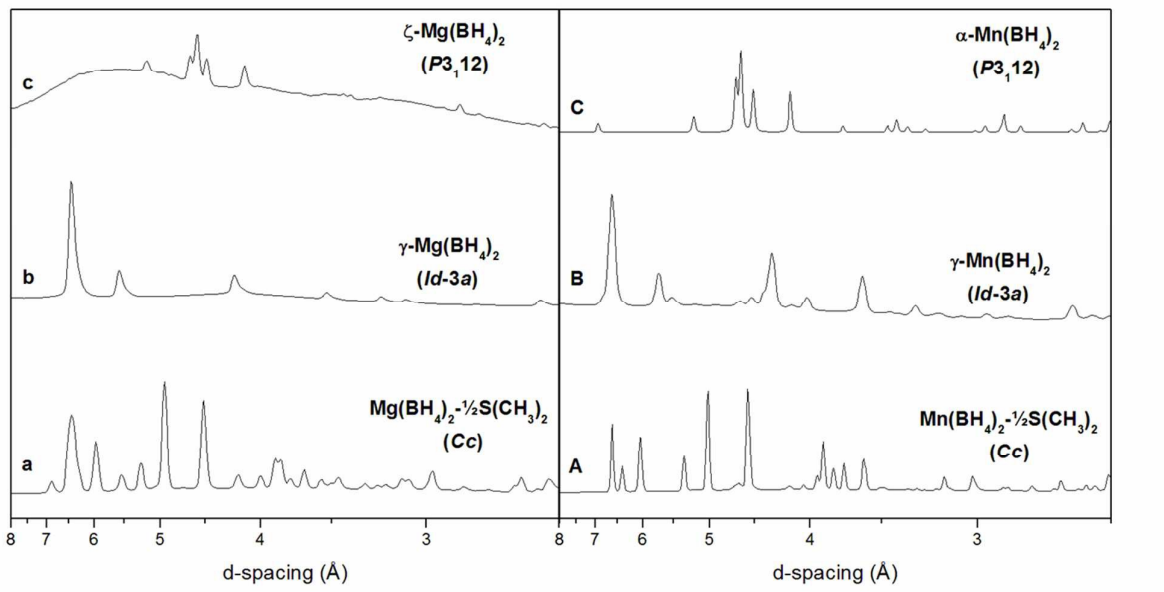

Figure 2. Powder X-ray diffraction patterns for $Mg(BH_4)_2$ and $Mn(BH_4)_2$ polymorphs: (left) (**a**) $Mg(BH_4)_2 \cdot ½S(CH_3)_2$, (**b**) γ-$Mg(BH_4)_2$, (**c**) ζ-$Mg(BH_4)_2$ shown in comparison to (right) (**A**) $Mn(BH_4)_2 \cdot ½S(CH_3)_2$, (**B**) γ-$Mn(BH_4)_2$ and (**C**) α-$Mn(BH_4)_2$. Experimental details of X-ray data for the $Mg(BH_4)_2$ polymorphs presented here are found in the supporting information.

Several manganese and magnesium borohydride polymorphs are isostructural and display similar diffraction patterns. The slightly larger manganese ion ($r(Mn^{2+})$ = 0.66 Å) compared to the magnesium ion ($r(Mg^{2+})$ = 0.57 Å) [52] accounts for a larger unit cell and thus a slight shift of diffraction patterns towards lower Bragg angles. The initially isolated solvate product $Mn(BH_4)_2 \cdot ½S(CH_3)_2$ (A) is transformed under vacuum at *RT* into γ-$Mn(BH_4)_2$ (B) upon prolonged treatment, while the magnesium analogue $Mg(BH_4)_2 \cdot ½S(CH_3)_2$ (a) transforms into its γ-$Mg(BH_4)_2$ polymorph (b) upon heating in vacuo much faster. Formation of α-$Mn(BH_4)_2$ (C) proceeds by heating of $Mn(BH_4)_2 \cdot ½S(CH_3)_2$ in vacuo. The structural parameters of the isostructural magnesium and manganese borohydride polymorphs are tabulated in Table 1 to provide an overview underlining their similarities.

Table 1. Structural parameters for the isostructural $Mn(BH_4)_2$ and $Mg(BH_4)_2$ polymorphs.

Compound	**Space Group**	**Cell Parameters**					
		(Å)	**β (°)**	***V* (Å^3)**	***Z***	***V/Z***	**Ref.**
$Mn(BH_4)_2 \cdot ½S(CH_3)_2$	*Cc*	*a* = 7.6914(4) *b* = 13.8731(8) *c* = 12.4278(7)	103.973(4)	1286.84(13)	4	321.71	- [a]
$Mg(BH_4)_2 \cdot ½S(CH_3)_2$	*Cc*	*a* = 7.6325(4) *b* = 13.8411(8) *c* = 12.4290(8)	103.833(3)	1274.94(13)	4	318.74	[39]
α-$Mn(BH_4)_2$	$P3_112$	*a* = 10.435(1) *c* = 10.835(2)	-	1021.8(3)	9	113.53	[32]
ζ-$Mg(BH_4)_2$	$P3_112$	*a* = 10.424(3) *c* = 10.729(5)	-	1009.7(7)	9	112.19	- [a]
γ-$Mn(BH_4)_2$	*Id*-3*a*	*a* = 16.2090	-	4258.6	24	177.44	- [a]
γ-$Mg(BH_4)_2$	*Id*-3*a*	*a* = 15.7575(16)	-	3912.6(7)	24	163.03	[39]

[a] This work.

Dalton Trans, 2014, revised 19332614_File000003_410109473.docx

Spectroscopic analysis of manganese and magnesium borohydride polymorphs.

$Mn(BH_4)_2 \cdot ½S(CH_3)_2$, γ-$Mn(BH_4)_2$ and α-$Mn(BH_4)_2$ were examined by ATR-FTIR, and compared to the corresponding spectra of magnesium borohydride (Figure 3).

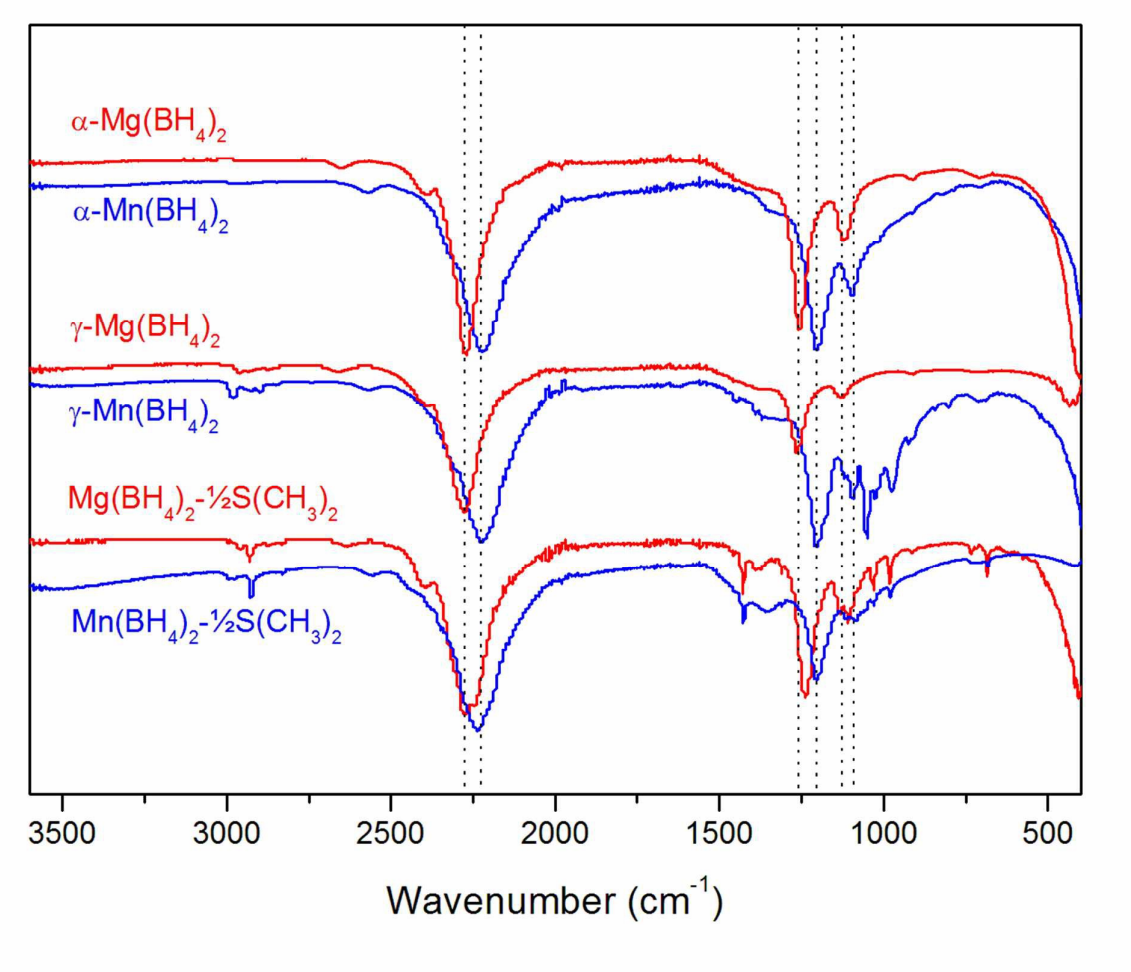

Figure 3. Infrared spectroscopy for manganese and magnesium borohydride polymorphs. Red; α-$Mg(BH_4)_2$ (top), γ-$Mg(BH_4)_2$ (middle), $Mg(BH_4)_2 \cdot ½S(CH_3)_2$ (bottom). Blue; α-$Mn(BH_4)_2$ (top), γ-$Mn(BH_4)_2$ (middle), $Mn(BH_4)_2 \cdot ½S(CH_3)_2$ (bottom). Dotted lines to guide the eye.

The spectrum for $Mn(BH_4)_2 \cdot ½S(CH_3)_2$ exhibits vibrational modes from both borohydride B-H and C-H bonds (stretching 2983 - 2848 cm^{-1} and bending 1424 - 683 cm^{-1}), the latter disappearing

gradually as the solvent is lost from RT to 110 °C. B-H stretching in $Mn(BH_4)_2$ is observed from 2600-2200 cm^{-1}, while further stretching, bending and combination bands are observed in the range from 1500 cm^{-1} and below. The close structural relation between magnesium and manganese borohydride is easily recognizable in Figure 3. It should be emphasized that the similarities are unique; seen in the perspective that spectra for other metal borohydrides are significantly different [53], thus underlining that these materials are structurally very much alike. Unidentified bands are observed in the spectra for γ-$Mn(BH_4)_2$. These bands could arise from residual solvent or amorphous impurities present.

Thermal decomposition behavior of manganese borohydride.

As seen from the temperature dependent *in situ* SR-PXD (Figure 4) $Mn(BH_4)_2 \cdot ½S(CH_3)_2$ transforms directly to α-$Mn(BH_4)_2$ in the temperature range 70 to 95 °C (see inset in Figure 4) while losing the solvated DMS.

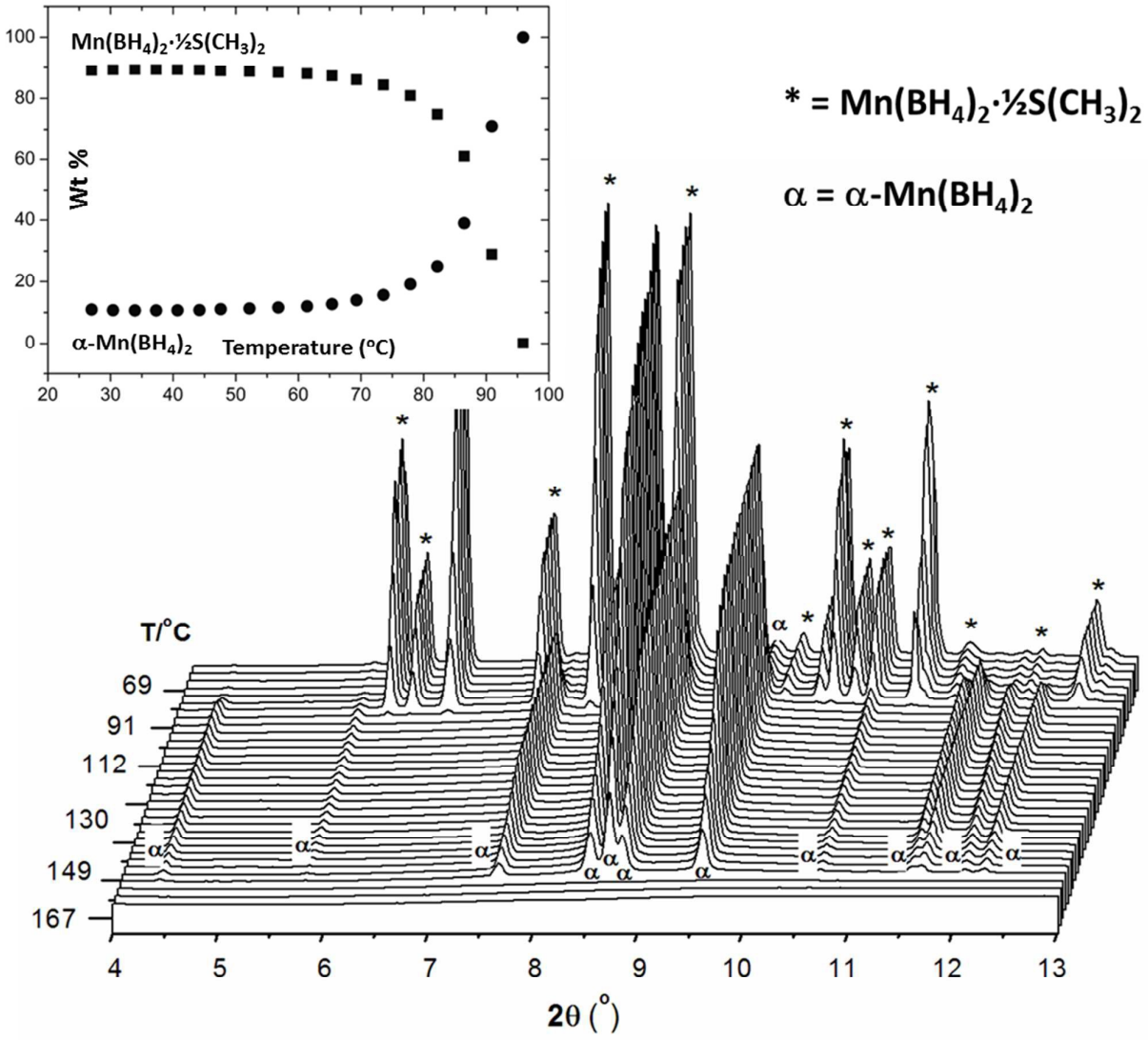

Figure 4. *In situ* synchrotron radiation powder X-ray diffraction measured from room temperature to 200 °C of $Mn(BH_4)_2 \cdot ½S(CH_3)_2$ (λ = 0.696713 Å, *p*(Ar) = 1 bar). **Inset:** Integrated intensities (wt%) of $Mn(BH_4)_2 \cdot ½S(CH_3)_2$ and α-$Mn(BH_4)_2$ as a function of temperature. Filled circles: α-$Mn(BH_4)_2$, filled squares: $Mn(BH_4)_2 \cdot ½S(CH_3)_2$.

Further heating results in the thermal decomposition of α-$Mn(BH_4)_2$ and loss of diffraction as no crystalline decomposition products were observed at any time.

Dalton Trans, 2014, revised 19332614_File000003_410109473.docx

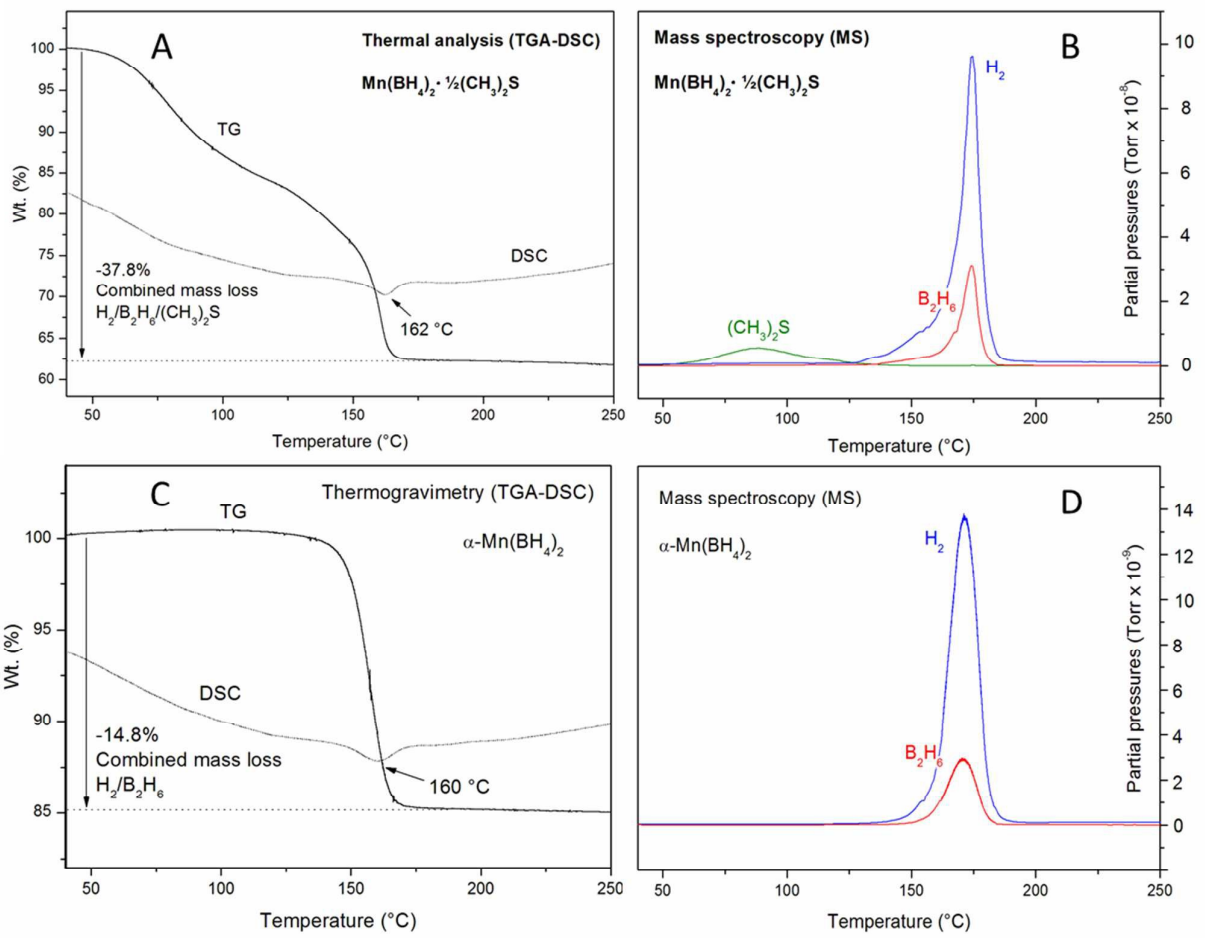

Figure 5. Thermogravimetry and differential scanning calorimetry (TGA-DSC, left, A, C) in combination with mass spectroscopy (MS, right, B, D) for $Mn(BH_4)_2 \cdot ½S(CH_3)_2$ (top) and α-$Mn(BH_4)_2$ (bottom). Mass spectroscopy data for H_2, B_2H_6 and $S(CH_3)_2$ ($\Delta T/\Delta t$ = 5 °C/min, p(Ar) = 1 bar).

For $Mn(BH_4)_2 \cdot ½S(CH_3)_2$ the TGA shows a total weight loss of 37.8 wt%, in two overlapping steps, in the temperature range 50 to 170 °C, see figure 5, A. The calculated contribution from loss of dimethylsulfide is 26.9 wt%. The remaining mass loss corresponds to hydrogen, $\rho_m(Mn(BH_4)_2)$ = 9.53 wt% H_2, and loss of some diborane. The decomposition of α-$Mn(BH_4)_2$ is seen as an endothermic event at ~160 °C in the DSC curves (Figure 5A and C) in good agreement with the *in situ* SR-PXD data (Figure 4). A mass loss of 14.8 wt%, in the temperature range 125 to 175 °C, is

observed for the sample of α-$Mn(BH_4)_2$ (Figure 5C), which corresponds well to the observations for the solvate. The mass spectroscopy data reveals the presence of a substantial amount of diborane in the evolved hydrogen. In lieu of accurate gas quantification methods, relating the experimentally observed weight loss of 10.9 wt% to a table of fixed H_2/B_2H_6 ratios provides a useful estimate of the relative ratio of H_2 and B_2H_6 (see supporting information). In this manner a ratio of H_2 to B_2H_6 of 16:1 is estimated. This is in contrast to previous observations made in a study involving nano-Ni doping of Li-Mn-B-H complexes, which were later proven to be $Mn(BH_4)_2$, wherein they observed a significantly higher proportion of hydrogen in the desorbed gases [27]. The decomposition products was suggested to be elemental boron and manganese metal for the reaction releasing mainly hydrogen. [45] Slightly different decomposition patterns were suggested in a study involving materials obtained from mechanochemical treatment of 2-3 equivalents of $LiBH_4$ and 1 equivalent $MnCl_2$ [54]. The following decomposition pathway was suggested (scheme 2);

$$2Mn(BH_4)_2 \rightarrow Mn + MnB_2 + 5H_2 + B_2H_6 \qquad (2)$$

however, this decomposition entails the loss of 22.4 wt% which is higher than our findings of 14.8 wt%. We further investigated the decomposition of α-$Mn(BH_4)_2$ by temperature dependent *in situ* SR-PXD experiments under different conditions; in vacuum (Figure S4.1a), under a backpressure of hydrogen ($p(H_2)$ = 10 bar, Figure S4.1b) and in argon (p(Ar) = 1 bar, Figure S4.1c). Depending on the conditions, α-$Mn(BH_4)_2$ is observed to decompose as early as 140 °C (vacuum), and up to 160 °C (p(Ar) = 1 bar) [55]. The decomposition of α-$Mn(BH_4)_2$ and $Mn(BH_4)_2{\cdot}½S(CH_3)_2$ at T > 125 °C follows the same pathway, i.e. TGA/DSC/MS results correspond to one another and *in situ* SR-PXD reveals amorphous decomposition products. *In situ* SR-PXD experiments were also conducted for γ-$Mn(BH_4)_2$ and diffraction disappears at T > 110 °C (p(Ar) = 1 bar, Figure S4.1d), giving rise to an amorphous hump in the background, similar to that observed for γ-$Mg(BH_4)_2$, i.e. heating the porous structure results in its collapse into amorphous $Mn(BH_4)_2$. Diffraction patterns measured at

RT after decomposition were not assigned to any known crystalline compounds (Figure S5.1). However, manganese metal, manganese borides and/or elemental boron may be involved in an overall reaction pathway for the decomposition of $Mn(BH_4)_2{\cdot}½S(CH_3)_2$ and $Mn(BH_4)_2$. Formation of polyboranes, such as $MnB_{12}H_{12}$, can also be envisioned on the basis of reports that diborane can react with $LiBH_4$ at elevated temperatures [56].

CONCLUSIONS

In this work we have demonstrated a solvent based synthesis method providing solvent and halide free $Mn(BH_4)_2$. The reaction affords a mixture of LiCl and $Mn(BH_4)_2$, from which three polymorphs of $Mn(BH_4)_2$ are extracted. The initially isolated product is a new solvate material, $Mn(BH_4)_2{\cdot}½S(CH_3)_2$, isostructural to $Mg(BH_4)_2{\cdot}½S(CH_3)_2$. The solvent can be removed upon treatment in vacuo at elevated temperatures, providing α-$Mn(BH_4)_2$, which is shown to be isostructural to a new $Mg(BH_4)_2$ polymorph denoted ζ-$Mg(BH_4)_2$. Gently extracting the solvent from $Mn(BH_4)_2{\cdot}½S(CH_3)_2$ and maintaining the structural integrity, yields another polymorph, γ-$Mn(BH_4)_2$ which is isostructural to γ-$Mg(BH_4)_2$ and provides a direct structural link between manganese and magnesium borohydrides. $Mn(BH_4)_2$ decomposes at temperatures significantly lower than $Mg(BH_4)_2$ (140 - 160 °C vs. 280 - 290 °C), which was extensively investigated. In addition, the discovery of a porous γ-$Mn(BH_4)_2$ polymorph may prompt further work on e.g. physisorption of H_2 in the porous cavities. Deducing detailed reaction schemes for the decomposition of $Mn(BH_4)_2$ under various conditions is highly desirable. This is particularly important for future, prospective work aiming at tailoring or tuning the properties towards rehydrogenating the material, especially considering the low decomposition temperature observed for this material.

ASSOCIATED CONTENT

Supporting Information.

Rietveld refinement plots, further experimental details, gas desorption quantification estimation methods, ex/*in situ* powder X-ray diffraction plots for decomposition reactions and crystal data from refined and calculated models as CIF files.

AUTHOR INFORMATION

Corresponding Author

*Tel.: +45 20745528 (B. R.), +45 87 15 59 39 (T. R. J.). Email: richter@chem.au.dk (B. R.), trj@chem.au.dk (T. R. J.)

Notes

The authors declare no competing financial interest.

ACKNOWLEDGEMENTS

The work was supported by the Danish National Research Foundation, Center for Materials Crystallography (DNRF93), The Danish Council for Strategic Research (project HyFillFast), and by the Danish Research Council for Nature and Universe (Danscatt). The access to beamtime at the synchrotron facilities MAX-II, Lund, Sweden in the research laboratory MAX-Lab, beam line I711 and at the Swiss-Norwegian Beam Lines (SNBL), European Synchrotron Radiation Facility (ESRF), Grenoble, France is gratefully acknowledged. We are grateful to the Carlsberg Foundation. We also acknowledge funding from the European Community's Seventh Framework Programme, The Fuel Cells and Hydrogen Joint Undertaking (FCH JU), project BOR4STORE (303428). Part of this work was supported by the COST Action MP1103 "Nanostructured materials for solid-state

hydrogen storage". DBR thanks the Carlsberg Foundation and the Villum Foundation for funding. We acknowledge the Fonds Spéciaux de Recherche (UCL) for the incoming postdoctoral fellowship co-funded by the Marie Curie actions of the European Commission granted to N.T. The authors thank FNRS for the financial support.

REFERENCES

References and Notes.

1. Sustainable Energy — without the hot air, David JC MacKay, UIT, CAMBRIDGE, Copyright David JC MacKay 2009. (Open access: www.withouthotair.com).

2. M. Felderhoff, C. Weidenthaler, R. von Helmolt, U. Eberle, *Phys. Chem. Chem. Phys*., 2007, **9**, 2643.

3. M. B. Ley, L. H. Jepsen, Y. -S. Lee, Y. W. Cho, J. B. von Colbe, M. Dornheim, M. Rokni, J. O. Jensen, M. Sloth, Y. Filinchuk, J. E. Jørgensen, F. Besenbacher, T. R. Jensen, *Materials Today*, 2014, **17**, 122-128.

4. L. H. Rude, T. K. Nielsen, D. B. Ravnsbæk, U. Bösenberg, M. B. Ley, B. Richter, L. M. Arnbjerg, M. Dornheim, Y. Filinchuk, F. Besenbacher, T. R. Jensen, *Phys. Status Solidi A*, 2011, **8**, 1754-1773.

5. S. Orimo, Y. Nakamori, J. R. Eliseo, A. Züttel, C.M. Jensen, *Chem. Rev.*, 2007, **107**, 4111–4132.

6. L. H. Jepsen, M. B. Ley, Y. -S. Lee, Y. W. Cho, M. Dornheim, J. O. Jensen, Y. Filinchuk, J. E. Jørgensen, F. Besenbacher, T. R. Jensen, *Materials Today*, 2014, **17**, 129-135.

7. D. B. Ravnsbæk, R. Černý, Y. Filinchuk, T. R. Jensen, *Z. Kristallographie*, 2010, **225**, 557–569.

8. P. Schouwink, M. B. Ley, T. R. Jensen, L. Smrčok, R. Černý, *Dalton Trans*, 2014, **43**, 7726–7733.

9. R. Černý, P. Schouwink, Y. Sadikin, K. Stare, L. Smrčok, B. Richter, T. R. Jensen, *Inorg. Chem.*, 2013, **52**, 9941−9947.

10. W. Grochala, P. P. Edwards, *Chem. Rev.* 2004, **104**, 1283–1315.

11. M. Paskevicius, M. B. Ley, D. A. Sheppard, T. R. Jensen, C. E. Buckley, *Phys. Chem. Chem. Phys.*, 2013, **15**, 19774.

12. J. J. Vajo, S. L. Skeith, F. Mertens, *J. Phys. Chem. B,* 2005, **109**, 3719–3722.

13. U. Bösenberg, S. Doppiu, L. Mosegaard, G. Barkhordarian, N. Eigen, A. Borgschulte, T. R. Jensen, Y. Cerenius, O. Gutfleisch, T. Klassen, M. Dornheim, R. Bormann, *Acta Mater*. 2007, **55**, 3951–3958.

14. J.J. Vajo, S. L. Skeith, *J. Phys. Chem. B,* 2005*,* **109**, 3719–3722.

15. T. K. Nielsen, U. Bösenberg, R. Gosalawit, M. Dornheim, Y. Cerenius, F. Besenbacher, T. R. Jensen, *ACS Nano*, 2010, **4**, 3903 - 3908.

16. T. K. Nielsen, P. Javadian, M. Polanski, F. Besenbacher, J. Bystrzycki, J. Skibsted, T. R. Jensen, *Nanoscale*, 2014, **6**, 599–607.

17. L. M. Arnbjerg, D. B. Ravnsbæk, Y. Filinchuk, R. T. Vang, Y. Cerenius, F. Besenbacher, J. E. Jørgensen, H. J. Jakobsen, T. R. Jensen, *Chem. Mater.*, 2009, **21**, 5772–5782.

18. L. H. Rude, Y. Filinchuk, M. H. Sørby, B. C. Hauback, F. Besenbacher, T. R. Jensen, *J. Phys. Chem. C*, 2011, **115**, 7768-7777.

19. E. A. Nickels, M. O. Jones, W. I. F. David, S. R. Johnson, R. L. Lowton, M. Sommariva, P. P. Edwards, *Angew. Chem., Int. Ed.*, 2008, **47**, 2817–2819.

20. D. Ravnsbæk, Y. Filinchuk, Y. Cerenius, H. J. Jakobsen, F. Besenbacher, J. Skibsted, T. R. Jensen, *Angew. Chem., Int. Ed.*, 2009, **48**, 6659-6663.

21. G. Severa, E. Rönnebro, C. M. Jensen, *Chem. Commun*., 2010, **46**, 421-423.

22. G. W. Schaeffer, J. S. Roscoe, A. C. Stewart, *J. Am. Chem. Soc*., 1956, **78**, 729–733.

23. R. Černý, G. Severa, D. B. Ravnsbæk, Y. Filinchuk, V. D'Anna, H. Hagemann, D. Haase, C. M. Jensen, T. R. Jensen, *J. Phys. Chem. C*, 2010, **114**, 1357.

24. T. J. Klingen, *Inorg. Chem.*, 1964, **7**, 1058.

25. H. M. Hoekstra, J. Katz, J. *J. Am. Chem. Soc.*, 1949, **71**, 2488.

26. L. H. Rude, M. Corno, P. Ugliengo, M. Baricco, Y. -S. Lee, Y. W. Cho, F. Besenbacher, J. Overgaard, T. R. Jensen, *J. Phys. Chem. C*, 2012, **116**, 20239−20245.

27. P. Choudhury, S. S. Srinivasan, V. R. Bhethanabotla, Y. Goswamib, K. McGrath, E. K. Stefanakos, *Int. J. Hydrogen Energy*, 2009, **34**, 6325-6334.

28. G. Severa, H. Hagemann, M. Longhini, J. W. Kaminski, T. A. Wesolowski, C. M. Jensen, *J. Phys. Chem. C*, 2010, **114**, 15516-15521.

29. E. Roedern, T. R. Jensen, *J. Phys. Chem. C*, 2014*,* **118**, 23567−23574.

30. O. Friedrichs, A. Borgschulte, S. Kato, F. Buchter, R. Gremaud, A. Remhof, A. Züttel, *Chem. Eur. J.*, 2009, **15**, 5531 – 5534.

31. V. D. Makhaev, A. P. Borisov, T. P. Gnilomedova, E. B. Lobkovskii, A. N. Chekhlov, *Bulletin of the Academy of Sciences of the USSR Division of Chemical Science*, 1987**, 36**, 1582–1586.

32. R. Černý, N. Penin, H. Hagemann, Y. Filinchuk, *J. Phys. Chem. C*, 2009, **113**, 9003-9007.

33. T. R. Jensen, T. K. Nielsen, Y. Filinchuk, J. E. Jørgensen, Y. Cerenius, E. M. Gray, C. J. Webb, *J. Appl. Cryst.*, 2010, **43**, 1456.

34. C. B. Mammen, T. Ursby, Y. Cerenius, M. Thunissen, J. Als-Nielsen, S. Larsen, A. Liljas, *Acta Physica Polonica. A*, 2002, **101**, 595-602.

35. Y. Cerenius, K. Stahl, L. A. Svensson, T. Ursby, A. Oskarsson, J. Albertsson, A. Liljas, *J. Synchrotron Radiat.*, 2000, **7**, 203-208.

36. A. P. Hammersley, S. O. Svensson, M. Hanfland, A. N. Fitch, D. Häusermann, *High Pressure Res.*, 1996, **14**, 235-248.

37. S. Vogel, L. Ehm, K. Knorr, G. Braun, *Adv. X-ray Anal.*, 2002, **45**, 31-33.

38. J. Rodriguez-Carvajal, *Physica B.*, 1993, **192**, 55.

39. Y. Filinchuk, B. Richter, T. R. Jensen, V. Dmitriev, D. Chernyshov, H. Hagemann, *Angew. Chem.*, *Int. Ed.*, 2011, **50**, 11162 – 11166.

40. W. I. F. David, S. K. Callear, M. O. Jones, P. C. Aeberhard, S. D. Culligan, A. H. Pohl, S. R. Johnson, K. R. Ryan, J. E. Parker, P. P. Edwards, C. J. Nuttall, A. Amieiro-Fonseca, *Phys. Chem. Chem. Phys*., 2012, **14**, 11800-11807.

41. V. N. Konoplev, *Russ. J. Inorg. Chem. (Transl. of Zh. Neorg. Khim.)*, 1980, **25**, 964.

42. J. Huot, D.B. Ravnsbæk, J. Zhang, F. Cuevas, M. Latroche, T.R. Jensen, *Prog. Mater. Sci.*, 2013, **58**, 30–75.

43. R. A. Varin, L. Zbroniec, M. Polanski, Y. Filinchuk, R. Černý, *Int. J. Hydrogen Energy*, 2012, **37**, 160556-16069.

44. R. Černý, N. Penin, V. D'Anna, H. Hagemann, E. Durand, J. Růžička, *Acta Mater.*, 2011, **59**, 5171-5180.

45. P. Choudhury, V. R. Bhethanabotla, E. Stefanakos, *J. Phys. Chem. C*, 2009, **113**, 13416-13424.

46. K. Chłopek, C. Frommen, A. Léon, O. Zabara, M. Fichtner, *J. Mater. Chem.*, 2007, **17**, 3465-3564.

47. D. A. Brandreth, M. C. Molstad, *Journal of Chemical & Engineering Data*, 1962, **7**, 449–450.

48. H. Hagemann, R. Černý, *Dalton Trans*., 2010, **39**, 6006–6012.

49. M. B. Ley, M. Paskevicius, P. Schouwink, B. Richter, D. A. Sheppard, C. E. Buckley, T. R. Jensen, *Dalton Trans*., 2014, **43**, 13333–13342.

50. T. D. Humphries, M. B. Ley, C. Frommen, K. T. Munroe, T. R. Jensen, B. C. Hauback, *J. Mater. Chem. A*, 2015, **3**, 691–698.

51. V. Ban, R. Černý, B. Richter, T. R. Jensen, C. J. Webb, Y. Filinchuk, *MH2012*, Poster MoP-33.

52. D. R. Lide, *CRC Handbook of Chemistry and Physics*, 88th ed., 2007-2008, pp. 12-11.

53. V. D'Anna, A. Spyratou, M. Sharma, H. Hagemann, *Spectrochimica Acta Part A: Molecular and Biomolecular Spectroscopy*, 2014, **128**, 902–906.

54. R. Liu, D. Reed, D. Book, *J. Alloys Compd.*, 2012, **515**, 32-38.

55. M. D. Riktor, M. H. Sørby, K. Chłopek, M. Fichtner, F. Buchter, A. Züttel, B. C. Hauback, *J. Mater. Chem.*, 2007, **17**, 4939-4942.

56. O. Friedrichs, A. Remhof, S.-J. Hwang, A. Züttel, *Chem. Mater.*, 2010, **22**, 3265–3268.

Table of content

Three manganese borohydride polymorphs are synthesized in solution and found to be structural analogues of three magnesium borohydride polymorphs.